TEC-00307-2024

High Precision Online MTPA Algorithm Considering Magnet Flux Parameter Mismatch for a PMa-SynRM

Dongyang Li, *Student Member, IEEE*, Shuo Wang, *Member, IEEE*, Chunyang Gu, *Member, IEEE*, Yuli Bao, *Member, IEEE*, Xiaochen Zhang, *Member, IEEE*, Chris Gerada, *Senior Member, IEEE*, and He Zhang, *Senior Member, IEEE*

Abstract— To improve the controlled current angle accuracy and reduce the copper loss for a Permanent Magnet assisted Synchronous Reluctance Machine (PMa-SynRM), this paper proposes an online Maximum Torque per Ampere (MTPA) control strategy based on Virtual High-Frequency Signal Injection (VHSI) to find its control current angle. The proposed method considers the nonlinear characteristics of the d- and q-axis inductance, d- and q-axis flux linkage, and permanent magnet flux. An error was identified in the mathematical determination of the MTPA control angle, stemming from the omission of the inductance's dependency on the current angle in the analysis. To solve the problem, an improved error supplementary control strategy considering permanent magnet flux mismatch was proposed, which features a lower calculation burden, less motor parameters information required, and higher precision. In this process, only permanent magnet flux information needs to be identified.

The proposed MTPA detection and its supplementary control scheme was analyzed from mathematical derivation and verified by experiments.

***Index Terms*—Permanent magnet-assisted synchronous reluctance machine, maximum torque per ampere, virtual high-frequency signal injection, error supplementation**

I. INTRODUCTION

PMa-SynRMs play a significant role spanning from academia to industry due to cost-effectiveness and independence on rare-earth materials, in contrast to Permanent Magnet Synchronous Machines (PMSMs) [1-3]. Furthermore, they exhibit superior efficiency and power factor when compared to both inductance machines (IMs) and non-PM Synchronous Reluctance Machines (SynRMs) [4]. Nevertheless, the presence of non-linear characteristics and parameter uncertainties, encompassing factors such as parameter variations, flux deviations, saturation, and cross-saturation, collectively contribute to the heightened challenge of achieving precise MTPA control [5]. For example, the temperature-dependent nature of the machine's equivalent resistance introduces the complexity to MTPA control [6]. In response to this issue, a growing number of researchers are actively exploring potential methodologies for determining optimal MTPA operating points [7-29].

The control strategies can be divided into three categories. In the direction of looking-up table (LUT) based control, the determination of MTPA current angle hinges upon the utilization of flux and inductance data. This necessitates a pre-built MTPA table, thereby reducing the computational load stemming from minimal calculation requisites [7]. However, the acquisition of data is not always available to engineers, as confidentiality shrouds certain machines during their production process. Meanwhile, the flux and inductance characteristics are subjected to drift due to machine aging, while inherent manufacturing process tolerance is unavoidable [8]. These factors collectively render the LUT approach unavailable and unreliable under specific circumstances. Ref [9-11] clarify that even accurate data does not eliminate control error in the MTPA angle. This highlights the limitations of using LUT based MTPA control in scenarios where high efficiency is crucial.

In reaction to this, [12] advances an online tracking scheme for MTPA control, obviating the demand for explicit inputs of machine parameters. However, it prolonged periods of calculation convergence when confronted with heavy-load operating scenarios. To eliminate this limitation, [13] proposed an augmented control methodology aimed to increase convergence rates. Nevertheless, it is noteworthy the supplementary method provides limited calculation convergence improvements according to simulations, in-depth analysis and experiments need be done for further verification.

Ref [14] introduced an MTPA tracking technique reliant on VHSI for IPMSM, wherein the MTPA control angle could be ascertained independent of flux variations and flux saturation. This control approach underwent validation within an 11 kW machine, culminating in an observed tracking error bound of under 0.5% in terms of current magnitude. Ref [15-16] presented a method employing pseudorandom frequency-switching signal injection. This procedure translated the constant-frequency harmonic current spectrum into a broad-frequency harmonic current spectrum. Nonetheless, the theoretical analysis of injected current frequency selection and feasibility remained unaddressed. Furthermore, considerations regarding the current sampling frequency and switching frequency were notably absent. Ref [17-18] improves the MTPA angle detection method through modifying the injected signals. The artificial intelligence algorithms were adopted in [19-20] to improve the accuracy of the MTPA control angle. To further research the influence of flux variation, flux and magnet saturation on the MTPA detection, improvements and research on modeling of IPM combining MTPA control were researched in [21-24]

Ref [25] proposed a signal injection based MTPA control scheme necessitating solely the DC bus current, leading to an enhancement in control topology, particularly relevant to cost-

sensitive applications. Ref [26] centered on flux weakening control hinging on the VHSI method, effectively combining the constant torque and flux weakening regions.

Ref [28] introduced an innovative vector space signal approach, negating the imperative for bandwidth considerations within the speed and current loops. Meanwhile, the paper investigates the MTPA angle errors via methodologies. Moreover, [29] advocated an extended signal injection control strategy, including considerations of the flux derivative term and subsequent estimation and compensation of the derivative component to mitigate errors, ultimately leading to a decrease in MTPA angle discrepancies. Additionally, Ref [9-11] and [27] directed its focus towards error analysis and a commensurate reduction in MTPA angle error. [11] presented an error compensation strategy reliant exclusively on the *q*-axis flux linkage. Notably, [10] devised an error compensation loop control paradigm necessitating no supplementary information for regulation. Nonetheless, it's essential to highlight that the assumption of constant value of magnet flux may not be suitable for some extreme working conditions and some materials. Meanwhile, cross-saturation was not considered. It means that the error still existed in the MTPA control process.

To further address these issues, this paper proposed an error supplementary control strategy to obtain a precise MTPA angle. The proposed control strategy only relies on the permanent magnet flux information of the magnet. In order to reduce the calculation burden, the flux linkage data is fitted with a polynomial. Through mathematic analysis, the calculated MTPA angle is coincided with the real MTPA angle. The main contributions are as follows:

a) An online MTPA control strategy was proposed based on VHSI which only relies on the permanent magnet flux of the machine. Compared to HSI based method, it brings less current distortion.

b) Error analysis was carried out to analyze between the control angle and real MTPA angle through mathematical differential equations.

c) An error supplementary loop was added to compensate for the MTPA detection error, in which only the information of permanent magnet flux in polynomial form is needed.

d) Simulations and experiments were carried out to verify the feasibility of the proposed control strategy.

The following part of the paper are organized as follows: Section I introduce the background of the research, research significance, and main research point of this paper. The mathematical model based on FEA data via the form of a LUT for PMa-SynRM was set up and an online MTPA detection method was carried out based on VHSI in Section II. Then, error analysis was carried out and compensated in the main control loop in Section III. In Section IV, the machine parameters and setting up of experiments were introduced. Meanwhile, experiments were carried out.

II. VHSI Based MTPA Control For PMa-SynRM

A. PMa-SynRM Modeling

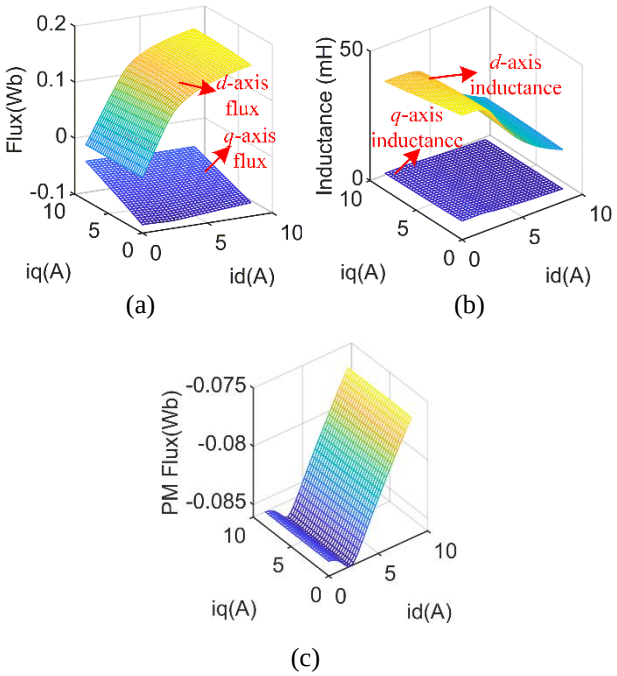

Fig. 1 Flux and inductance characteristics of the PMa-SynRM (a) *d*- and *q*-axis flux with different *d*- and *q*-axis current; (b) *d*- and *q*-axis inductance with different *d*- and *q*-axis current; (c) permanent magnet flux with different *d*- and *q*-axis current

The voltage equation in *d*- and *q*-axis is adopted in (1) considering cross saturation [12].

$$\begin{cases} u_{\mathrm{d}} = (R_{\mathrm{s}} + \Delta R_s) i_{\mathrm{d}} + \dfrac{\mathrm{d}\left(L_{\mathrm{d}} i_{\mathrm{d}} + L_{\mathrm{dq}} i_{\mathrm{q}}\right)}{\mathrm{dt}} \\ \qquad -\omega_{\mathrm{e}}\left(L_{\mathrm{q}} i_{\mathrm{q}} + L_{\mathrm{qd}} i_{\mathrm{d}} - \psi_{\mathrm{pm}}\right) \\ u_{\mathrm{q}} = (R_{\mathrm{s}} + \Delta R_s) i_{\mathrm{q}} + \dfrac{\mathrm{d}\left(L_{\mathrm{q}} i_{\mathrm{q}} + L_{\mathrm{qd}} i_{\mathrm{d}} - \psi_{\mathrm{pm}}\right)}{\mathrm{dt}} \\ \qquad +\omega_{\mathrm{e}}\left(L_{\mathrm{d}} i_{\mathrm{d}} + L_{\mathrm{dq}} i_{\mathrm{q}}\right) \end{cases} \tag{1}$$

where, u_{d} and u_{q} is the voltage of *d*- and *q*-axis, respectively; R_{s} is the stator resistance in 25℃; $\triangle R_{\mathrm{s}}$ is the resistance variation caused by temperature changes; i_{d}, and i_{q} is the *d*- and *q*-axis current, respectively; L_{d} and L_{q} is the *d*- and *q*-axis inductance linkage, respectively; L_{dq} and L_{qd} is the *d*- and *q*-axis cross inductance caused by *q*- and *d*-axis current; ω_e is the electrical speed of the PMa-SynRM; ψ_{pm} is the flux of the permanent magnet.

Cross-saturation, self-saturation, and inductance variations of the machine were considered in the machine modelling. Fig. 1 shows the inductance and flux of the PMa-SynRM obtained from the Finite element analysis (FEA). According to the *d*- and *q*-axis inductance of the machine in (b), *d*- and *q*-axis inductance is largely influenced by *d*- and *q*-axis current, respectively. It should be noted that the *d*-axis inductance is affected by both the *d*-axis current and the *q*-axis current.

The flux along the *d*- and *q*-axis could also be used for further verification. In Fig. 1(a), as the current increases, the

flux linkage tends to remain unchanged, which means that the magnetic saturation greatly influences the flux and inductance. The change in *q*-axis inductance has the same trend as the change in *d*-axis inductance.

In [6], the calculation of the MTPA method is based on a fixed value of *d*- and *q*-axis current. However, inductance variation, magnetic saturation, and cross-saturation need to be considered for this machine for the calculation of the MTPA working trajectory, which will be discussed in the following section.

B. Characteristics of MTPA Working Point

Fig. 2(a) shows that different pairs of *d*- and *q*-axis currents could be obtained with the same current limit. The same output torque could be obtained with different pairs of *d*- and *q*-axis, in which minimized stator current could be satisfied in point A. As shown in Fig. 2(c), as the current angle increases, the stator current varies to guarantee the same output torque. As depicted in A, the minimized current could be obtained, and the angle need to be calculated to reduce the copper loss. As shown in Fig. 2(d), the rated torque could be obtained in point A, and the control angle is about 0.8 rad. In this paper, the goal is to find the control angle of A to reduce the copper loss.

In general, the MTPA working point could be obtained with the computational method. A minimum current magnitude could be obtained in this solution (i_d, i_q pair). By using MTPA, the following constrained optimization problem could be obtained as shown in (2).

$$\begin{cases} \text{minimize } |i_s| = \sqrt{i_d^2 + i_q^2} \\ \text{subject to } \dfrac{3}{2}p(\psi_d i_q - \psi_q i_d) = T_e \end{cases} \tag{2}$$

where

$$\begin{cases} i_d = |i_s| \cos\theta \\ i_q = |i_s| \sin\theta \end{cases} \tag{3}$$

where $|i_s|$ is the current vector magnitude, θ is the angle between current vector i_s and the *d*-axis direction, The torque could be obtained as (4).

$$T_e = \frac{3p}{2}\left[\psi_{pm} i_s \cos\theta + \frac{1}{2}(L_d - L_q) i_s^2 \sin 2\theta + L_{dq} i_s^2 \sin^2\theta - L_{qd} i_s^2 \cos^2\theta\right] \tag{4}$$

Denote L_{dt} as the equivalent inductance of the L_d and L_{dq} for *d*-axis; L_{qt} as the equivalent inductance of the L_q and L_{qd} for *q*-axis obtained from FEA. As a result of (4), the *d*- and *q*-axis currents should comply with (5) under the MTPA condition.

$$\theta = \arcsin\left(\frac{-\psi_{pm} + \sqrt{\psi_{pm}^2 + 8(L_{dt} - L_{qt})^2 i_s^2}}{4(L_{dt} - L_{qt}) i_s}\right) \tag{5}$$

From (5), the MTPA angle is decided by L_{dt}, L_{qt}, and ψ_{pm}, in which these parameters are variables. Therefore, directly calculating the current angle is computation consuming. A method based on LUTs can be applied, but preparing the necessary data requires extensive experimentation and significant time investment.

To address this issue, an online MTPA control method based on VSIM is proposed. This method generates the MTPA angle by injecting a high-frequency small amplitude sinusoidal signal and controlling the proportional term of the torque derivative to zero. It considers the flux cross saturation and does not rely on nonlinear parameters, making it more convenient than the LUT-based method.

In addition, the derivation term of torque to current control angle was not considered in (5). So, the current control angle exists an error compared to the real applications. In this paper, this error was considered and compensated for in the later theoretical analysis and experiments.

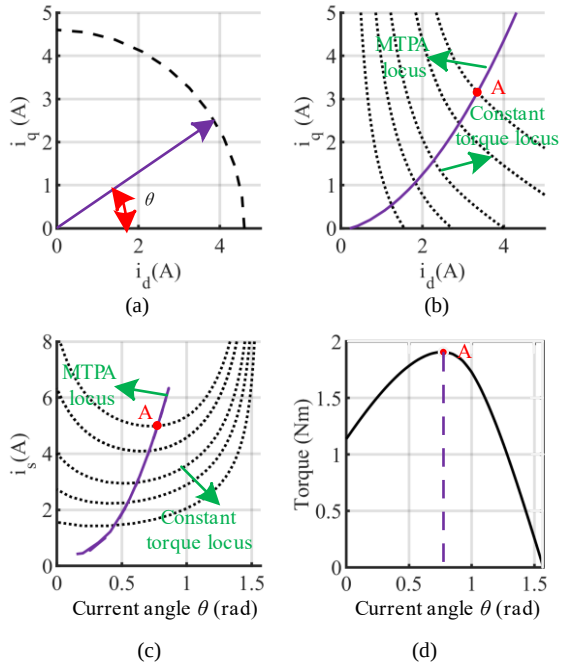

Fig. 2 Relationship between the current and torque for the PMa-SynRM (a) *d*- and *q*-axis current with stator current limit; (b) torque locus with different *d*- and *q*-axis current; (c) torque locus with different stator current and current angle; (d) output torque with different current angle.

C. Power Analysis with Injected Current

Due to the inherent challenges in calculating or measuring torque accurately in industrial applications, the MTPA tracking method presented in this paper employs a novel approach based on signal injection to evaluate $\partial T_e/\partial\theta$, the proposed method involves injecting a high-frequency, small signal into the system to facilitate the estimation process. So, the current angle θ with the injected signal could be obtained as (6).

$$\theta = \theta_{avg} + \theta_h = \theta_{avg} + A_{mag}\sin(f_h \times 2\pi t) \tag{6}$$

where θ is the real current angle in the control process, θ_{avg} is the current angle in base frequency, and θ_h is the injected current angle; A_{mag} is the magnitude of the injected signal; f_h is the frequency of the injected signal; t represents time unit.

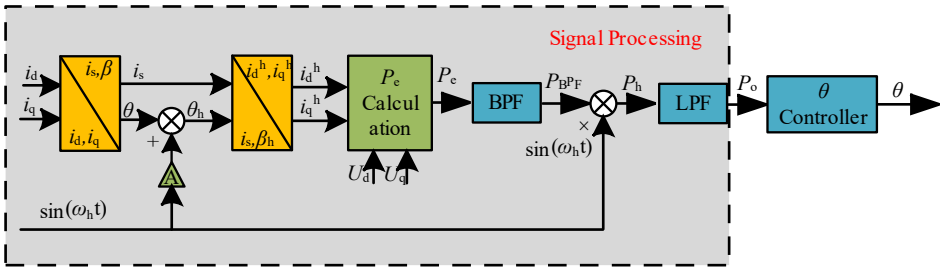

Fig.3 Signal processing to get the MTPA criterion.

(7) and (8) could be obtained according to (3) and (6).

$$\begin{aligned} i_{dh} &= i_s\cos\left(\theta_{avg} + A_{mag}\sin\omega_h t\right) \\ &\approx i_s\cos\theta_{avg} - i_s A_{mag}\sin\theta_{avg}\sin\omega_h t \\ &= i_{db} + i_{di} \end{aligned} \tag{7}$$

$$\begin{aligned} i_{qh} &= i_s\sin\left(\theta_{avg} + A_{mag}\sin\omega_h t\right) \\ &\approx i_s\sin\theta_{avg} + i_s A_{mag}\cos\theta_{avg}\sin\omega_h t \\ &= i_{qb} + i_{qi} \end{aligned} \tag{8}$$

In real applications, the injected current angle will influence the *d*- and *q*-axis current, which may further cause speed loop oscillation and torque fluctuation. To minimize further impact on the speed control loop, or to reduce any additional influence on the speed control loop, the injected current frequency is selected as 400 Hz.

The choice of the frequency and the depends on the noise level and the dynamic requirements of the system.[14]. Typically, the current angle is considered a low-frequency signal, while the high-frequency signal is related to the IGBT switching frequency. Therefore, the injected signal must lie within this range. If the injection frequency is too low, signal extraction becomes difficult, requiring a lower low-pass filter cutoff, which negatively impacts the system's dynamic response. Conversely, if the frequency is too high, it becomes hard to distinguish from high-frequency noise and increases the MCU's computational burden, as higher frequencies mean more points need to be calculated within the same time frame. Balancing these considerations, a 400Hz signal was chosen. As for the torque fluctuation, the variation could be neglected using the Taylor series expansion [14].

$$\begin{aligned} P_e &= P_{copper} + P_{reactive} + P_{mech} \\ &= \frac{3}{2}\left[R_s\left(i_d^2 + i_q^2\right) + \Delta R_s\left(i_d^2 + i_q^2\right) + L_d\frac{di_d}{dt}i_d\right. \\ &+ L_q\frac{di_q}{dt}i_q + L_{qd}\frac{di_q}{dt}i_d + L_{dq}\frac{di_d}{dt}i_q + \frac{d\psi_{pm}}{dt}i_q \\ &\left.+ \omega_m\psi_{pm}i_d + \omega_m\left(L_d - L_q\right)i_d i_q + L_{dq}i_q^2 - L_{qd}i_d^2\right] \end{aligned} \tag{9}$$

$$P_{copper} = (R_s + \Delta R_s)i_s^2 = R_s i_s^2 + \Delta R_s i_s^2 \tag{10}$$

$$\begin{aligned} P_{reactive} &= \frac{3}{2}\left[\left(L_{qd}\cos^2\theta_{avg} - L_{dq}\sin^2\theta_{avg}\right)\right. \\ &\left.- \frac{1}{2}\left(L_d - L_q\right)\sin2\theta_{avg}\right]i_s^2 A_{mag}\omega_h\cos\omega_h t + \\ &\frac{3}{4}\left(L_d\sin^2\theta_{avg} + L_q\cos^2\theta_{avg} + \frac{1}{2}\left(L_{dq} - L_{qd}\right)\sin2\theta_{avg}\right) \\ &\times i_s^2 A_{mag}^2\omega_h\sin2\omega_h t \end{aligned} \tag{11}$$

$$\begin{aligned} P_{mech} &\approx \frac{3}{2}\omega_m\left[\frac{1}{2}\left(L_d - L_q\right)i_s^2\sin2\theta_{avg} - \right. \\ &\left.\psi_{pm}i_s\cos\theta_{avg} + L_{dq}i_s^2\sin^2\theta_{avg}\right] \\ &-L_{qd}i_s^2\cos^2\theta_{avg} + \frac{3}{2}\left[\psi_{pm}\sin\theta_{avg} + \left(L_d - L_q\right)\right] \\ &i_S\cos2\theta_{avg} \times i_s\omega_m A_{mag}\sin\omega_h t \\ &+ \frac{3}{8}\omega_m\left(L_d - L_q\right)i_s^2 A_{mag}^2\sin2\theta_{avg}\cos2\omega_h t \\ &+ \frac{3}{4}\left(L_{dq}\cos^2\theta_{avg} - L_{qd}\sin^2\theta_{avg}\right)\omega_m i_s^2 A_{mag}^2 \\ &- \frac{3}{4}\left(L_{dq}\cos^2\theta_{avg} - L_{qd}\sin^2\theta_{avg}\right)\omega_m i_s^2 A_{mag}^2\cos2\omega_h t \\ &+ \frac{3}{2}\left(L_{dq} + L_{qd}\right)\omega_m i_s^2\sin2\theta_{avg}A_{mag}\sin\omega_h t \end{aligned} \tag{12}$$

Since the torque features a linear relationship with the output power at a fixed speed. The torque with respect to current angle could be analyzed through input power as shown in (9)-(12).

D. Evaluation of $\partial T_e/\partial\theta$ for MTPA Tracking

To further evaluate and extract the mechanical power, to get the MTPA operating point, the filters described in Fig. 3 were used to get the output power from the input power. In the proposed control structure in Fig.3, the output power P_o as (13), which proved to have a linear relationship with the torque, could be extracted. Through the first bandpass filter, the copper loss part could be eliminated because no high-frequency signal is contained in this part. Although the resistance varies with the temperature, it could be regarded as a fixed value in the electrical power sampling process because it is a slowly varying component. After the bandpass filter, the signal was then plus $\sin(\omega_h t)$ to eliminate the orthogonal component, in which the reactive power part could be eliminated. After that, a low-pass filter was used to extract the low-frequency part of the mechanical power and the output P_o, which could be expressed in (13).

$$\begin{aligned} P_o = \frac{1}{2}A_{mag}\omega_m i_s\left[-\psi_{pm}\sin\theta\right. \\ + \left(L_d - L_q\right)i_s\cos2\theta \\ \left.+ \left(L_{dq} + L_{qd}\right)i_s\sin2\theta\right] \end{aligned} \tag{13}$$

According to (4), (14) could be obtained.

$$\begin{aligned} \frac{\partial T_e}{\partial\theta} = \frac{3}{2}pi_s\left[-\psi_{pm}\sin\theta + \left(L_d - L_q\right)i_s\cos2\theta + \left(L_{dq}\right.\right. \\ \left.\left.+ L_{qd}\right)i_s\sin2\theta\right] \end{aligned} \tag{14}$$

In (14), the derivation term concerning permanent magnet flux, *d*- and *q*-axis flux were not considered. The $\partial \mathrm{T_e}/\partial\theta$ could be expressed as (15) if this part were considered.

$$\begin{aligned}\frac{\partial T_e}{\partial\theta}=\frac{3p}{2}i_s[&-\psi_{\mathrm{pm}}\sin\theta+\left(L_{\mathrm{d}}-L_{\mathrm{q}}\right)i_{\mathrm{s}}\cos2\theta\\&+(L_{\mathrm{dq}}+L_{\mathrm{qd}})i_{\mathrm{s}}\sin2\theta\\&+\left(\frac{\partial L_{\mathrm{d}}}{\partial\theta}-\frac{\partial L_{\mathrm{q}}}{\partial\theta}\right)i_s\frac{1}{2}\sin2\theta-\frac{\partial\psi_{pm}\left(\theta_{\mathrm{avg}}\right)}{\partial\theta}\cos\theta\\&-\frac{\partial L_{\mathrm{dq}}}{2\,\partial\theta}i_s\cos2\theta-\frac{\partial L_{\mathrm{qd}}}{2\,\partial\theta}i_s\cos2\theta]\end{aligned}\tag{15}$$

The extracted P_{o} features a linear relationship with the torque assuming the speed is fixed, which means the MTPA question could be simplified to control P_{o} to 0.

To ensure effective injection of high frequency current, a high frequency supplementary current loop is needed to have a better performance [14], which will not be discussed in this paper.

III. MTPA Control Error Analysis and Compensation

A. MTPA Control Error Analysis

According to (1), (16) and (17) could be obtained:

$$\psi_{\mathrm{pm}}-L_{\mathrm{qd}}i_{\mathrm{d}}=L_{\mathrm{q}}i_{\mathrm{q}}-\psi_q=L_{\mathrm{q}}i_{\mathrm{q}}+\frac{u_{\mathrm{d}}-R_{\mathrm{s}}i_{\mathrm{d}}}{\omega_{\mathrm{e}}}\tag{16}$$

$$(L_{\mathrm{d}}-L_{\mathrm{q}})i_{\mathrm{d}}+L_{\mathrm{dq}}i_{\mathrm{q}}=\frac{u_{\mathrm{q}}-R_{\mathrm{s}}i_{\mathrm{q}}}{\omega_{\mathrm{e}}}-L_{\mathrm{q}}i_{\mathrm{d}}\tag{17}$$

Substituting (16), (17) and (3) into (4) leads to (18)

$$\begin{aligned}T_{\mathrm{e1}}=\frac{3}{2}p\Big[&\left(\frac{u_{\mathrm{q}}-R_{\mathrm{s}}i_{\mathrm{q}}}{\omega_{\mathrm{e}}i_d}-L_{\mathrm{q}}\right)i_di_q+(L_{\mathrm{q}}i_{\mathrm{q}}\\&+\frac{u_d-R_si_d}{\omega_{\mathrm{e}}})i_d\Big]\end{aligned}\tag{18}$$

The significance of (18) is that only L_{q} is required for the output torque evaluation and calculation, which less parameters are needed compared to (4).

The above equations analyze the situation that small angle signals were not injected. However, the injected signals expressed in (7) and (8) must be evaluated, in which (19) could be obtained.

$$\begin{aligned}T_{\mathrm{eh}}=\frac{3}{2}p\Big[&\left(\frac{u_{\mathrm{q}}-R_{\mathrm{s}}i_{\mathrm{q}}}{\omega_{\mathrm{e}}i_{\mathrm{d}}}-L_{\mathrm{q}}\right)i_{\mathrm{dh}}i_{\mathrm{qh}}+(L_{\mathrm{q}}i_{\mathrm{q}}\\&+\frac{u_{\mathrm{d}}-R_{\mathrm{s}}i_{\mathrm{d}}}{\omega_{\mathrm{e}}})i_{\mathrm{dh}}\Big]\end{aligned}\tag{19}$$

To simplify the calculation process, (18) could be simplified as (20).

$$T_{\mathrm{e1}}=\frac{3}{2}p\left[(a_1+a_2i_{\mathrm{d}})i_{\mathrm{d}}+(b_1+b_2\frac{i_{\mathrm{q}}}{i_{\mathrm{d}}})i_{\mathrm{d}}i_{\mathrm{q}}\right]\tag{20}$$

where, $a_1=\psi_{\mathrm{pm}}$;$a_2=-L_{\mathrm{qd}}$; $b_1=L_{\mathrm{d}}-L_{\mathrm{q}}$; $b_2=L_{\mathrm{dq}}$.

According to (19), (21) could be obtained.

$$\begin{aligned}T_{\mathrm{eh}}=\frac{3}{2}p\Big[&\frac{u_{\mathrm{d}}-R_{\mathrm{s}}i_{\mathrm{d}}}{\omega_{\mathrm{e}}}+L_{\mathrm{q}}\left(i_{\mathrm{q}}-i_{\mathrm{qh}}\right)\\&+\frac{u_{\mathrm{q}}-R_{\mathrm{s}}i_{\mathrm{q}}}{\omega_{\mathrm{e}}i_{\mathrm{d}}}i_{\mathrm{qh}}\Big]i_{\mathrm{dh}}\end{aligned}\tag{21}$$

Assuming that $i_{\mathrm{q}}\approx i_{\mathrm{qh}}$, $L_{\mathrm{q}}\left(i_{\mathrm{q}}-i_{\mathrm{qh}}\right)$ could be ignored and (22) could be get:

$$T_{\mathrm{eh}}\approx\frac{3}{2}p\left[\frac{u_{\mathrm{d}}-R_{\mathrm{s}}i_{\mathrm{d}}}{\omega_{\mathrm{e}}}+\frac{u_{\mathrm{q}}-R_{\mathrm{s}}i_{\mathrm{q}}}{\omega_{\mathrm{e}}i_{\mathrm{d}}}i_{\mathrm{qh}}\right]i_{\mathrm{dh}}\tag{22}$$

Simplify (22), we get:

$$T_{\mathrm{eh}}\approx\frac{3}{2}p\left[-ci_{\mathrm{dh}}+(d_1+d_2\frac{i_{\mathrm{q}}}{i_{\mathrm{d}}})i_{\mathrm{dh}}i_{\mathrm{qh}}\right]\tag{23}$$

where, $c=-(L_{\mathrm{q}}i_{\mathrm{q}}-a_2i_{\mathrm{d}}(i_{\mathrm{qh}}/i_{\mathrm{q}})-a_1)$, and $d_1=L_{\mathrm{d}}$; $d_2=b_2=L_{\mathrm{dq}}$

According to (18) and (20), (24) and (25) could be obtained:

$$\begin{aligned}\frac{\partial T_{\mathrm{e1}}}{\partial\theta}=\frac{3}{2}p[&-a_1i_{\mathrm{s}}\sin\theta+b_1i_s^2\cos2\theta+(b_2\\&-a_2)i_s^2\sin2\theta]\end{aligned}\tag{24}$$

$$\begin{aligned}\frac{\partial T_{\mathrm{e1}}}{\partial\theta}=\frac{3}{2}p\big[&-\psi_{\mathrm{pm}}i_{\mathrm{s}}\sin\theta+(L_{\mathrm{d}}-L_{\mathrm{q}})i_s^2\cos2\theta+(L_{\mathrm{dq}}\\&+L_{\mathrm{dq}})i_s^2\sin2\theta\big]\end{aligned}\tag{25}$$

(24) and (25) describes the situation that the online MTPA control strategy where the injected signals were not considered. However, the influence of the injected signal needs to be considered. (26) and (27) describe the derivation of torque with respect to angle where the injected angle was considered.

$$\begin{aligned}\frac{\partial T_{\mathrm{eh}}}{\partial\theta}=\frac{3}{2}p\big[&-a_1i_{\mathrm{s}}\sin\theta+b_1i_s^2\cos2\theta+(b_2\\&-a_2)i_s^2\sin2\theta-L_{\mathrm{qd}}\mathrm{i}_d^2-L_{\mathrm{qd}}\mathrm{i}_d^3/i_{\mathrm{q}}\big]\end{aligned}\tag{26}$$

$$\begin{aligned}\frac{\partial T_{\mathrm{eh}}}{\partial\theta}=\frac{3}{2}p\big[&-\psi_{\mathrm{pm}}i_{\mathrm{s}}\sin\theta+(L_{\mathrm{d}}-L_{\mathrm{q}})i_s^2\cos2\theta+(L_{\mathrm{dq}}\\&+L_{\mathrm{dq}})i_s^2\sin2\theta+(L_{\mathrm{dq}}\\&+L_{\mathrm{dq}})i_s^2\sin2\theta-L_{\mathrm{qd}}\mathrm{i}_d^2-L_{\mathrm{qd}}\mathrm{i}_d^3/i_{\mathrm{q}}\big]\end{aligned}\tag{27}$$

In (15), the deviation of the torque to angle is considered, while this part was not considered in the MTPA online detection part. It is obvious that an error existed in the proposed online signal injection based MTPA control strategy. In the following part, this error will be analyzed and compensated. (28) describes the error where the injected signal was not considered while (29) depicts the situation in the real signal injection process.

$$\begin{aligned}error_{\mathrm{L}}=&\frac{\partial T_{\mathrm{e}}}{\partial\theta}-\frac{\partial T_{\mathrm{e1}}}{\partial\theta}=\\&\frac{3}{2}pi_{\mathrm{s}}(\left(\frac{\partial L_{\mathrm{d}}}{\partial\theta}-\frac{\partial L_{\mathrm{q}}}{\partial\theta}\right)i_{\mathrm{s}}\frac{1}{2}\sin2\theta-\frac{\partial\psi_{\mathrm{pm}}}{\partial\theta}\cos\theta\\&-\frac{\partial L_{\mathrm{dq}}}{2\,\partial\theta}i_s\cos2\theta-\frac{\partial L_{\mathrm{qd}}}{2\,\partial\theta}i_s\cos2\theta)\end{aligned}\tag{28}$$

$$\begin{aligned}error_{\mathrm{h}}=&\frac{\partial T_{\mathrm{e}}}{\partial\theta}-\frac{\partial T_{\mathrm{eh}}}{\partial\theta}=\\&\tfrac{3}{2}pi_{\mathrm{s}}(\left(\tfrac{\partial L_d}{\partial\theta}-\tfrac{\partial L_q}{\partial\theta}\right)i_{\mathrm{s}}\tfrac{1}{2}\sin2\theta-\tfrac{\partial\psi_{\mathrm{pm}}}{\partial\theta}\cos\theta-\\&\tfrac{\partial L_{\mathrm{dq}}}{2\,\partial\theta}i_s\cos2\theta-\tfrac{\partial L_{\mathrm{qd}}}{2\,\partial\theta}i_s\cos2\theta-L_{\mathrm{q}}i_{\mathrm{d}}^2-L_{\mathrm{qd}}\mathrm{i}_d^3/i_{\mathrm{q}})\end{aligned}\tag{29}$$

B. Error Compensation

From the above analysis expressed in (28) and (29), an error existed with the proposed signal injection method. It is hard to calculate the error directly because it is not easy to calculate the differential part and the parameters are unknown. Since $\partial T_{\mathrm{eh}}/\partial\theta$ comes from T_{eh}, it can be observed that the mechanism of the signal processing from T_{eh} to $\partial T_{\mathrm{eh}}/\partial\theta$ is a derivative operation, where T_{eh} to $\partial T_{\mathrm{eh}}/\partial\theta$ could be calculated in Fig.3 with the same principle using the relationship between power and torque. Likewise, the error present in equation (29) can be derived by computing the derivative of an additional

function relative to the MTPA control angle. Consequently, this paper introduces a novel error formulation predicated on the construction of an underlying function associated with the error inherent in equation (29). The resultant mathematical expression is presented as follows:

$$T_{error} = \frac{3}{2}p[-\psi_{\mathrm{pm}}i_{\mathrm{d}} - L_{\mathrm{q}}i_{\mathrm{d}}i_{\mathrm{qh}} - L_{\mathrm{qd}}\mathrm{i}_d^2 + L_{\mathrm{d}}i_{\mathrm{d}}i_{\mathrm{q}} + L_{\mathrm{dq}}\mathrm{i}_q^2] \quad (30)$$

where

$$-\frac{\partial\psi_{\mathrm{pm}}}{\partial\theta}i_{\mathrm{d}} = -\left(\partial\psi_{\mathrm{pm}}i_{\mathrm{d}}\right)'\Big|_{\theta} \quad (31)$$

$$-\frac{\partial L_{\mathrm{q}}}{\partial\theta}i_{\mathrm{d}}i_{\mathrm{q}} - L_{\mathrm{q}}\mathrm{i}_{\mathrm{d}}^2 - \frac{\partial L_{\mathrm{qd}}}{2}\mathrm{i}_s^2 - \frac{\partial L_{\mathrm{qd}}}{2\,\partial\theta}\mathrm{i}_s^2\cos 2\theta - \frac{L_{\mathrm{qd}}\mathrm{i}_d^3}{i_{\mathrm{q}}} = \left(-L_{\mathrm{q}}i_{\mathrm{d}}i_{\mathrm{qh}} - L_{\mathrm{qd}}\mathrm{i}_d^2\right)'\Big|_{\theta} \quad (32)$$

$$\frac{\partial L_{\mathrm{d}}}{\partial\theta}i_{\mathrm{d}}i_{\mathrm{q}} + \frac{\partial L_{\mathrm{dq}}}{2}\mathrm{i}_s^2 - \frac{\partial L_{\mathrm{dq}}}{2\,\partial\theta}\mathrm{i}_s^2\cos 2\theta = \left(L_{\mathrm{d}}i_{\mathrm{d}}i_{\mathrm{q}} + L_{\mathrm{dq}}\mathrm{i}_q^2\right)'\Big|_{\theta} \quad (33)$$

In (30), a new compensation equation was proposed and used to compensate the error caused by the MTPA signal injection method. However, the information of the machine including *d*- and *q*-axis permanent magnet flux need to be known to calculate this part. To further simplify the problem, (34) could be obtained according to (1) and (31).

$$T_{error} = \frac{3}{2}p[-\psi_{\mathrm{pm}}i_{\mathrm{d}} + \frac{(u_d - R_{\mathrm{s}}i_{\mathrm{d}})i_{\mathrm{d}}i_{\mathrm{qh}}}{\omega_{\mathrm{e}}i_{\mathrm{q}}} + \frac{(u_q - R_{\mathrm{s}}i_{\mathrm{q}})i_{\mathrm{q}}}{\omega_{\mathrm{e}}}] \quad (34)$$

In (34), only resistor of the machine and permanent magnet flux are needed to get the torque error, in which resistor is easily obtained and considers to be temperature independent in the controlling process because the resistance is a slow varying parameter and could be regarded as a fixed value in the power extraction process. As for the permanent magnet flux, the variation could be observed from Fig.1. The variation of the flux varies about 10% because of the cross saturation of the PMa-SynRM and it cannot be neglected. From the above analysis, the error will be compensated if the permanent magnet flux could be obtained. To solve the above problem, the permanent magnet flux will be analyzed and fitted in the next section.

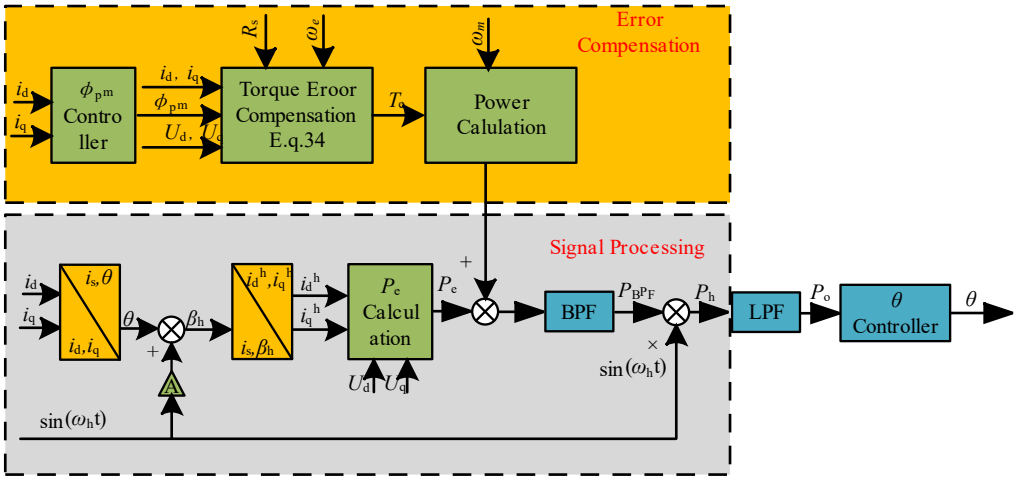

Fig.4 Overall control diagram

C. Modelling of Permanent Magnet Flux and Overall Control

As discussed above, Fig.4 shows the overall control diagram of the system. In the first step, the permanent magnet flux of the machine was obtained from the fitted polynomial. The fitted data is more accurate to the real value if the points of FEA data is not dense enough. Furthermore, the permanent magnet flux data of PMa-SynRM is more acceptable compared to the *d*-and *q*- axis flux data and could be obtained from the material manual.

Next, the error of the torque was obtained from (34). After that, the torque was translated in the form of the power and this part was compensated to the MTPA detection part. The error was calculated and compensated for by the control system. Meanwhile, the variation of the permanent magnate flux is considered and fitted to get a better control performance.

As shown in Fig.1, three sets of 31×31 flux linkage data are obtained from the FEA software. To solve the mentioned problem, the permanent magnet flux needs to be further learned and modelled. As shown in Fig.1(c), the magnet flux will be influenced by the *d*-axis current because of the cross saturation. Meanwhile, the *q*-axis current has little influence on the magnet flux. So, the magnet flux linkage could be fitted as a polynomial and the accuracy will be more accurate with the increasing of the order. However, the calculation will be more complicated. To balance the calculation time and accuracy, the magnet flux could be expressed as (35).

$$\hat{\psi}_{pm} = p_0 + p_1 i_d + p_2 \mathrm{i}_d^2 + p_3 \mathrm{i}_d^3 + p_4 \mathrm{i}_d^4 \quad (35)$$

where, p_0, p_1, p_2, p_3, p_4 are coefficients of the polynomial.

In real applications, 31×31 flux linkage data is not always acceptable. To address this issue, only five sets of data are needed to get a satisfactory polynomial function for the proposed fitting method. This data could be obtained from the experiments using the method proposed in [30]. To get the parameters of the polynomial, the least squares method (LSM) is used [30]. Meanwhile, five sets of data are used to get the polynomial and error analysis is carried out as shown in Fig.5.

From the above analysis in Fig.6, the average errors are

1.2%. For the permanent magnate flux, it is precise enough to describe the variation of magnate flux in the changing of working condition.

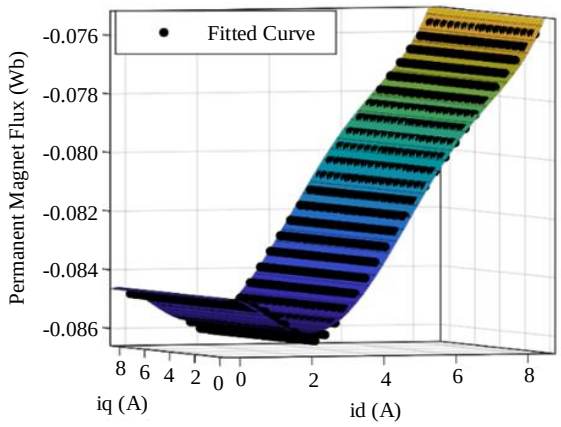

Fig.5. Performance of the proposed polynomial function

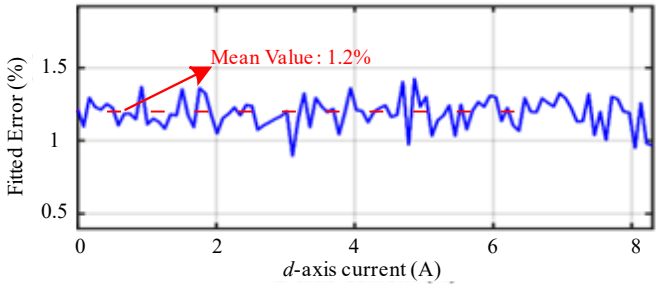

Fig.6. Error analysis of the proposed polynomial function

IV. Simulations and Experiments

A. Machine Parameters

To verify the feasibility of the proposed algorithm, the method was verified in a PMa-SynRM with a rated load of 1.9Nm and the rated speed of 2700 rpm. In addition, the parameters of inductance and flux are not a linear one. The nonlinear characteristics of the machine need to be paid attention to. The parameters of the PMa-SynRM are shown-in Table I in a detail way.

Table I. PMa-SynRM Parameters

Symbol	Definition	Values with unit
n	rated speed	2,700 rpm
T_e	rated torque	1.9 Nm
i_{ab}, i_{bc}, i_{ca}	rated current (RMS)	3.265 A
u_a, u_b, u_c	rated voltage (RMS)	110.0 V
p	pole pairs	2
L_d	d-axis inductance	Shown in Fig. 2(b)
L_q	q-axis inductance	Shown in Fig. 2(b)
R_s	winding resistance	1.028,4 Ohm
φ_{pm}	rotor flux linkage	0.084,83 Wb
E_{coef}	electromotive force coefficient (RMS)	0.02176 V/rpm
J	rotation inertia	3.296×10^{-4} kg.m^2

B. Setup of Control Platform

Experimental tests were carried out in this paper to verify the feasibility of the algorithm. Throughout the entire system, the control part and the drive part were integrated onto a single circuit board based on the STM32-F303 platform.

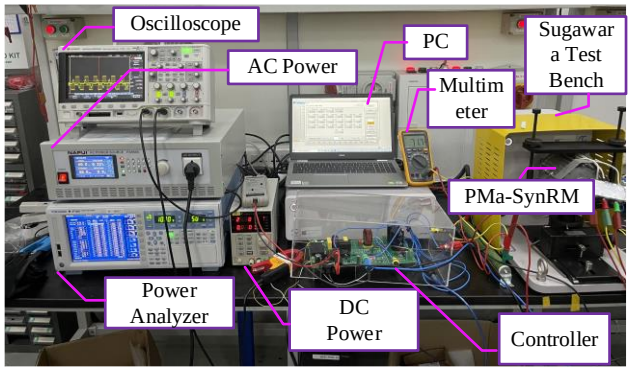

Fig.7 Hardware platform for the PMa-SynRM

Fig.7 illustrates the main experimental platform, which mainly consists of the Sugawara test bench for loading and unloading, and the YAKOGAWA power analyzer is used for the three-phase voltage and current data acquisition. Simultaneously, oscilloscopes were used to measure voltages and currents. For the power supply part of the board, AC power was used. Furthermore, STM32F303 micro-controller was used to achieve the proposed algorithm and the power module is STG series with 15A as peak current. Table II shows the software configuration.

Table II. PMa-SynRM Parameters

Specification	Value
Injection Signal Frequency	400 Hz
Amplitude of Injected Current	5% of Sampling Current
Sampling Frequency	4 kHz
LPF Cutoff Frequency	10 Hz
BPF Cutoff Frequency	400 Hz

In the filter design, a 400Hz band-pass filter and a 10Hz low-pass filter were chosen. The selection of the low pass filter cutoff frequency is critical for the system's stability. The system's dynamic response worsens if the cutoff frequency is too low, increasing the angle convergence time and thereby affecting the system's convergence time and stability. Conversely, if the low-pass filter cutoff frequency is too high, it leads to larger angle fluctuations, negatively impacting the system's steady-state performance.

Given that the injected frequency in our system is 400Hz, achieving optimal performance typically requires setting the low pass filter cutoff frequency to a maximum of 200Hz. After thorough analysis and experimentation, considering both system stability and response speed, a 10Hz cutoff frequency for the low-pass filter was the most suitable choice for the design.

C. Experiments Results for Proposed Compensation

In this experimental section, the objective is to monitor the MTPA characteristics at 2700 rpm, while the command torque is incrementally adjusted from 0 Nm to 1.9 Nm with steps of 0.2 Nm. Fig.9 outlines the MTPA locus obtained experimentally in the half-rated load and rated load. This

figure juxtaposes the tracking outcomes of the proposed error compensation method, which verifies the feasibility of the control strategy.

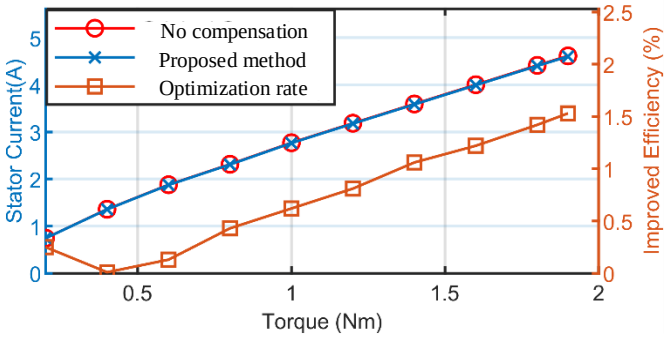

Fig.8 Performance of the proposed supplementation control strategy

To verify the improvement of the proposed compensation control method, the experiments subjected to two tracking methodologies, which refers to VHSI with compensation and no compensation link, operating at steady-state conditions were carried out. The MTPA locus points are derived from the mean values of the measured currents at these operating points. A notable observation is the significant variance in the magnitude of currents required by the no compensation method and its compensated counterpart. A comparative analysis of these two tracking methodologies is presented in Table III. The optimization rate is defined as (36) to evaluate the improvements performance of the proposed control strategy.

$$r = \frac{i_s(\text{ no compensation}) - i_s(\text{ proposed })}{I_s(\text{ no compensation})} 100\% \qquad (36)$$

Table III Comparation between original signal injection method and the proposed compensation method

Torque (Nm)	Original Current (A)	Compensation Current (A)	Optimization Rate
0.2	0.7457	0.7438	0.25%
0.4	1.3593	1.3559	0.01%
0.6	1.8791	1.8744	0.13%
0.8	2.3138	2.3080	0.43%
1.0	2.7706	2.7637	0.62%
1.2	3.1845	3.1765	0.81%
1.4	3.5931	3.5841	1.06%
1.6	4.0026	3.9926	1.22%
1.8	4.4131	4.4021	1.42%
1.9	4.6133	4.6018	1.53%

Table III and Fig.8 shows the experiments results of the proposed supplementation control strategy compared to the no compensation experiments set. The proposed method features a smaller current amplitude in the same working condition, thereby the efficiency was improved. Notably, the improvement is most significant when the torques are elevated, achieving an optimization rate as high as 1.53%, which is because the cross-saturation phenomenon is more severe in heavy loads.

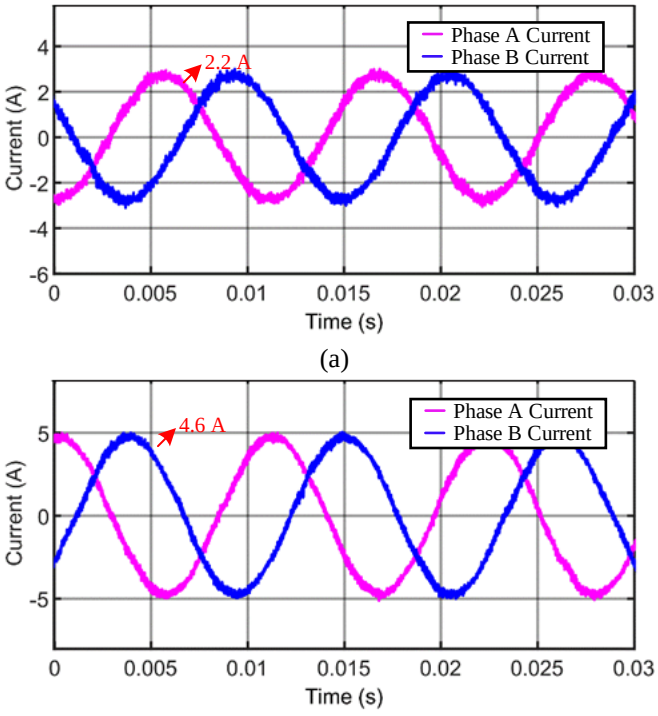

Fig.9 Phase current with the proposed MTPA compensation method (a) half-rated load working condition; (b)rated load working condition.

In the test experiments process, the three-phase current is measured from both the oscilloscope and the power analyzer. Fig.9 shows the phase current of the rated working condition and half-rated working condition, in which it could be observed that it reaches the steady state working condition and the magnitude of the current remains unchanged in a limited time.

The experiments show that the half-rated current and the rated current is around 2.6 A and 4.7A, respectively, which is consistent with theoretical analysis. Meanwhile, the phase angle between phase A and phase B is around 120 degrees, which verified the feasibility of the control strategy.

D. Analysis on the Influence of the Temperature

To ascertain the impact of resistance fluctuations attributable to thermal variations, experimental investigations were conducted under two distinct thermal regimes: a 'cold' temperature setting, typically operational for durations less than one minute, and a 'hot' temperature condition, with operational spans exceeding fifteen minutes. The 'cold' temperature scenario typically denotes a lower winding temperature, approximately 25℃, representing the initial or ambient state of the windings. Conversely, the 'hot' temperature scenario corresponds to an elevated winding temperature, contingent upon the design parameters of the machinery. This higher temperature, usually in the vicinity of 85℃, is observed under conditions of thermal equilibrium [31].

Fig.10 shows the theoretical value of the MTPA and the MTPA locus determined by the proposed control method in

1350 rpm and 2700rpm under the 'cold' machine conditions and Fig.11 shows the MTPA locus in 'hot' machine conditions.

In the comparative analyses presented in Fig.10 and Fig.11,

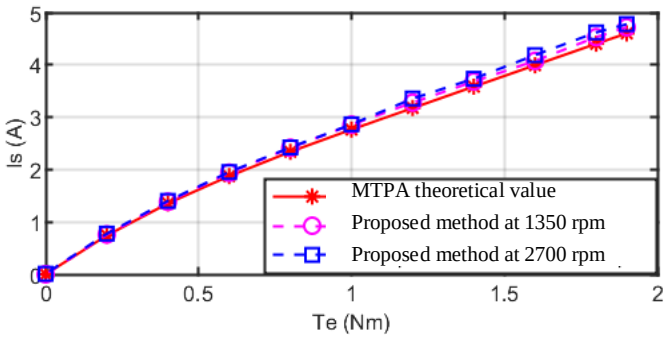

Fig. 10 Proposed MTPA method in cold machine condition

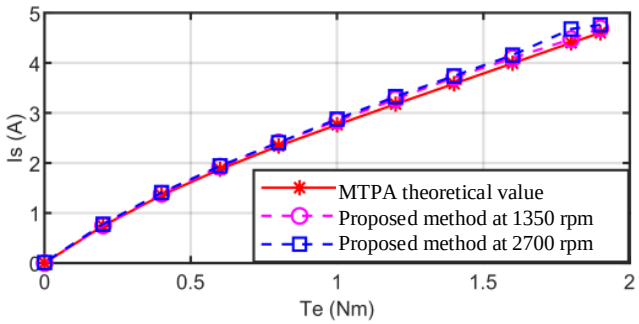

Fig.11 Proposed MTPA method in hot machine condition

which assess different operational scenarios, it is observed that the MTPA operating point ascertained through the proposed methodology exhibits negligible deviation. This minimal variation is attributed to the gradual nature of resistance change. These experimental results reveal the robustness of the proposed method to fluctuations in resistance. Meanwhile, it could be observed that the stator current in 1350 rpm and 2700 rpm is not perfect match in the experiments. This is mainly due to the following reasons: a) the designed low pass filter features different performance in different frequencies for the current, which leads to a different control sensibility for different speed; b) the iron loss is not the same in different speed, which was not considered in this paper [32-34]. c) The stable temperature of the motor is not the same at different power ratings, leading to a variation in the resistance.

E. Performance of the MTPA tracking

Fig 12 shows the load disturbance from 0 Nm to 1.9 Nm and 1.9 Nm to 0 Nm with a step load at 2700 rpm. Fig12 (a) shows the feedback of the *d*- and *q*-axis current while Fig12 (b) shows the given torque. The proposed control strategy could be convergence in a limited time. Generally, it depends on the speed loop and current loop, the PI controller was specially designed, and 0.5 s convergence time could be achieved [25-27].

Meanwhile, it could be observed in Fig (12) that the current control angle gets to a steady state in a limited time because of the *d*- and *q*-axis current remained unchanged in a limited time in the steady-state working condition. This verifies the feasibility of the proposed control strategy. Furthermore, with the increasing of the torque, the current control angle increases to meet MTPA requirements.

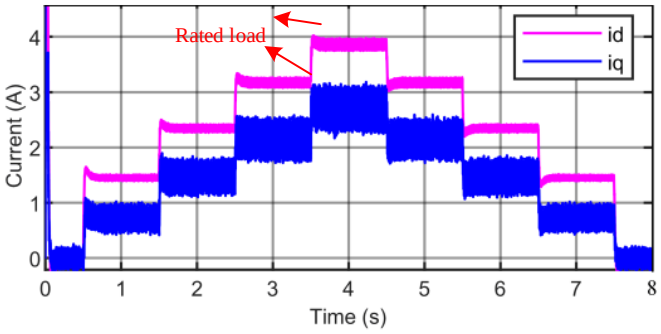

(a)

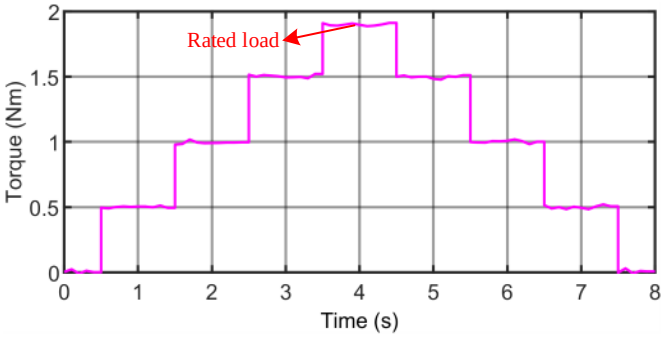

(b)

Fig. 12 *d*- and *q*-axis current under the whole working condition (a) *d*- and *q*-axis feedback current; (b) given torque.

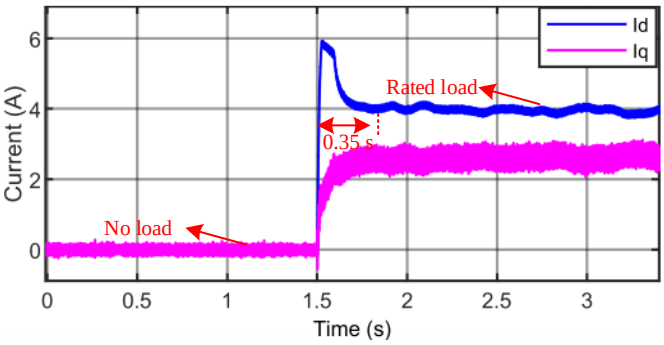

(a)

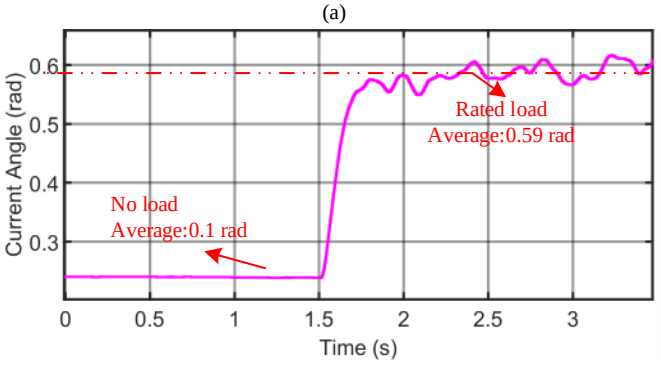

(b)

Fig.13 Step load from 0 Nm– 1.9 Nm. (a) *d*- and *q*-axis current response (b) MTPA control angle response

In Fig.13, the MTPA angle reaches stability within 0.5 seconds, and it fluctuates around 0.59 rads because the

functions of the low pass filter. It should be noticed that the convergence process only influences the efficiency of the machine, but not influences the stability of the machine because the derivation of the current angle is relevant small. It could also be found that the control angle for the no load condition is around 0.1 rads. This is because that the current amplitude in no load condition is very small, which is 0 A considering no damping situation. In this way, the current angle has little influence for the theoretical analysis. But for the experiments, small electrical output torque should be provided to overcome the damping friction of the system. In this way, a small MTPA control angle is observed for the control in no load condition.

Fig.14 illustrates the transition of the speed reference from 1350 rpm to 2700 rpm under a half-rated load. Concurrently, it is evident that the *d*- and *q*-axis current loops stabilize within 0.5 seconds to reach a stable condition. However, it only takes 0.09s for the current loop to reach the steady state. This implies that the currents exhibit minimal variation despite the fluctuating current angle throughout the process. Evidence from these experiments confirms that both the current control loop and the current angle control loop achieve stability within a predetermined timeframe, thereby validating the effectiveness of the proposed control strategy.

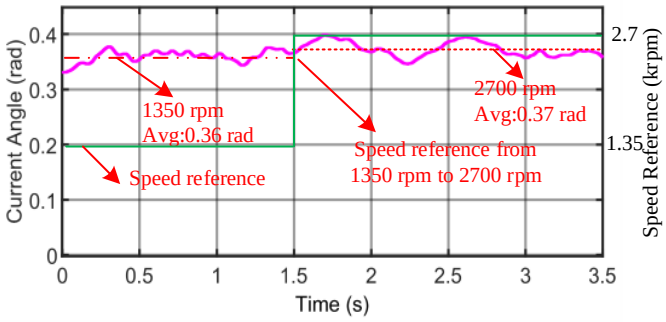

(a)

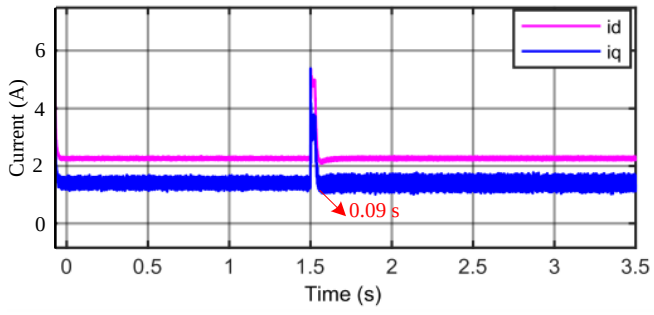

(b)

Fig. 14 Step speed reference variation from 1350 rpm to 2700 rpm (a) speed reference and current control angle (b) *d*- and *q*-axis current

The experimental setup under investigation utilizes a small power PMa-SynRM as its controlled object. It is important to note that the applicability of the proposed control methodology remains consistent irrespective of the motor's power rating, whether high or low. In the context of larger motors, a notable characteristic is the increased magnitude of the stator current. The absence of real signal injection into the stator currents allows the proposed approach to precisely track the MTPA points with less harmonica, concurrently facilitating a reduction in the stator current's amplitude. Consequently, the proposed strategy demonstrates good robustness and effectiveness. Future research endeavors will focus on reducing the reliability of the permanent magnet flux information and extending this methodology to high power motors, exploring its applicability and potential refinements in such contexts.

V. Conclusion

This paper introduced an innovative approach aimed at increasing the MTPA control accuracy and the efficiency for PMa-SynRMs. The proposed VHSI based online MTPA control strategy considers the permanent magnet flux mismatch and improves the accuracy of MTPA control angle through experiments.

Mathematical analysis revealed that there was a discrepancy compared to the actual MTPA due to the omission of the differentiation of inductance concerning the current angle. Consequently, a supplementary control strategy was introduced to address this issue. This supplementary control method offers several advantages, including low computational overhead, minimal reliance on motor parameters, and high precision.

Through rigorous mathematical derivation and validation via experiments, the proposed MTPA detection and supplementary control scheme have been demonstrated to be effective in improving the performance of PMa-SynRM systems, in which a maximum of 1.52% improvements in rated load and 0.62% improvements in half rated load could be achieved. This research represents a significant step forward in the field of PMa-SynRMs, offering a practical and efficient approach to optimize their operation.

References

[1] S. S. R. Bonthu, A. Arafat and S. Choi, "Comparisons of Rare-Earth and Rare-Earth-Free External Rotor Permanent Magnet Assisted Synchronous Reluctance Motors," in IEEE Transactions on Industrial Electronics, vol. 64, no. 12, pp. 9729-9738, Dec. 2017, doi: 10.1109/TIE.2017.2711580.

[2] C. López-Torres, A. Garcia, J. -R. Riba, G. Lux and L. Romeral, "Computationally Efficient Design and Optimization Approach of PMa-SynRM in Frequent Operating Torque–Speed Range," in IEEE Transactions on Energy Conversion, vol. 33, no. 4, pp. 1776-1786, Dec. 2018, doi: 10.1109/TEC.2018.2831249

[3] B. Wang, L. Luo, W. Hua, M. Cheng and S. Niu, "High Performance and Strong Fault Tolerant Triple 3-Phase PMA-SynRM With Star-Delta Windings," in IEEE Transactions on Energy Conversion, vol. 37, no. 3, pp. 1977-1986, Sept. 2022, doi: 10.1109/TEC.2022.3157471.

[4] P. Niazi and H. A. Toliyat, "Online Parameter Estimation of Permanent-Magnet Assisted Synchronous Reluctance Motor," in IEEE Transactions on Industry Applications, vol. 43, no. 2, pp. 609-615, March-april 2007, doi: 10.1109/TIA.2006.890021.

[5] A. Consoli, G. Scarcella, G. Scelba and A. Testa, "Steady-State and Transient Operation of IPMSMs Under Maximum-Torque-per-Ampere Control," in IEEE Transactions on Industry Applications, vol. 46, no. 1, pp. 121-129, Jan.-feb. 2010, doi: 10.1109/TIA.2009.2036665.

[6] K. Huang, W. Peng, C. Lai and G. Feng, "Efficient Maximum Torque Per Ampere (MTPA) Control of Interior PMSM Using Sparse Bayesian Based Offline Data-Driven Model With Online Magnet Temperature Compensation," in IEEE Transactions on Power Electronics, vol. 38, no. 4, pp. 5192-5203, April 2023, doi: 10.1109/TPEL.2022.3230052.

[7] G. Feng, C. Lai, Y. Han and N. C. Kar, "Fast Maximum Torque Per Ampere (MTPA) Angle Detection for Interior PMSMs Using Online Polynomial Curve Fitting," in IEEE Transactions on Power Electronics, vol. 37, no. 2, pp. 2045-2056, Feb. 2022, doi: 10.1109/TPEL.2021.3109112.

[8] C. Gong, L. Ding, Y. Li, X. Wu and X. Zhang, "Flux Observation Transfer-Based Inductance Identification Technique for Precise FCS-MPCC Used in Surface-Mounted PMSMs," in IEEE Transactions on Power Electronics, vol. 38, no. 4, pp. 4241-4245, April 2023, doi: 10.1109/TPEL.2023.3235269.

[9] T. Inoue, Y. Inoue, S. Morimoto and M. Sanada, "Maximum Torque Per Ampere Control of a Direct Torque-Controlled PMSM in a Stator Flux Linkage Synchronous Frame," in IEEE Transactions on Industry Applications, vol. 52, no. 3, pp. 2360-2367, May-June 2016, doi: 10.1109/TIA.2016.2531618.

[10] Z. Han, J. Liu, W. Yang, D. B. Pinhal, N. Reiland and D. Gerling, "Improved Online Maximum-Torque-Per-Ampere Algorithm for Speed Controlled Interior Permanent Magnet Synchronous Machine," in IEEE Transactions on Industrial Electronics, vol. 67, no. 5, pp. 3398-3408, May 2020, doi: 10.1109/TIE.2019.2918471.

[11] T. Sun, M. Koç and J. Wang, "MTPA Control of IPMSM Drives Based on Virtual Signal Injection Considering Machine Parameter Variations," in IEEE Transactions on Industrial Electronics, vol. 65, no. 8, pp. 6089-6098, Aug. 2018, doi: 10.1109/TIE.2017.2784409.

[12] G. Feng, C. Lai, X. Tan and N. C. Kar, "Maximum-Torque-per-Square-Ampere Control for Interior PMSMs Considering Cross-Saturation Inductances," in IEEE Transactions on Transportation Electrification, vol. 7, no. 3, pp. 1482-1492, Sept. 2021, doi: 10.1109/TTE.2021.3059238.

[13] D. -H. Kim and S. -H. Kim, "Modified Gradient Descent Algorithm Based Maximum Torque Per Ampere Control of PMSMs," 2021 24th International Conference on Electrical Machines and Systems (ICEMS), Gyeongju, Korea, Republic of, 2021, pp. 1736-1741, doi: 10.23919/ICEMS52562.2021.9634592.

[14] S. Kim, Y. -D. Yoon, S. -K. Sul and K. Ide, "Maximum Torque per Ampere (MTPA) Control of an IPM Machine Based on Signal Injection Considering Inductance Saturation," in IEEE Transactions on Power Electronics, vol. 28, no. 1, pp. 488-497, Jan. 2013, doi: 10.1109/TPEL.2012.2195203.

[15] K. Li, T. Sun, J. Liang, M. Koc and Y. Zhou, "Automatic MTPA Control for IPMSM Drives Based on Pseudorandomly Reversed Fixed-Frequency Sinusoidal Signal Injection," in IEEE Transactions on Industrial Electronics, vol. 71, no. 7, pp. 6863-6874, July 2024, doi: 10.1109/TIE.2023.3301523.

[16] Li K, Sun T, Jiang F, Feng W, Li H. MTPA Control for IPMSM Drives Based on Pseudorandom Frequency-Switching Sinusoidal Signal Injection. Machines. 2022 Mar 25;10(4):231.

[17] J. Xia, Y. Guo, Z. Li, J. Jatskevich and X. Zhang, "Step-Signal-Injection-Based Robust MTPA Operation Strategy for Interior Permanent Magnet Synchronous Machines," in IEEE Transactions on Energy Conversion, vol. 34, no. 4, pp. 2052-2061, Dec. 2019, doi: 10.1109/TEC.2019.2932455.

[18] X. Zhou, Y. Zhou, H. Wang, M. Lu, F. Zeng and Y. Yu, "An Improved MTPA Control Based on Amplitude-Adjustable Square Wave Injection," in IEEE Transactions on Energy Conversion, vol. 35, no. 2, pp. 956-965, June 2020, doi: 10.1109/TEC.2020.2968737.

[19] Y. A. . -R. I. Mohamed and T. K. Lee, "Adaptive self-tuning MTPA vector controller for IPMSM drive system," in IEEE Transactions on Energy Conversion, vol. 21, no. 3, pp. 636-644, Sept. 2006, doi: 10.1109/TEC.2006.878243.

[20] F. -J. Lin, Y. -T. Liu and W. -A. Yu, "Power Perturbation Based MTPA With an Online Tuning Speed Controller for an IPMSM Drive System," in IEEE Transactions on Industrial Electronics, vol. 65, no. 5, pp. 3677-3687, May 2018, doi: 10.1109/TIE.2017.2762634.

[21] G. Feng, C. Lai, Y. Han and N. C. Kar, "Fast Maximum Torque Per Ampere (MTPA) Angle Detection for Interior PMSMs Using Online Polynomial Curve Fitting," in IEEE Transactions on Power Electronics, vol. 37, no. 2, pp. 2045-2056, Feb. 2022, doi: 10.1109/TPEL.2021.3109112.

[22] A. Accetta, M. Cirrincione, M. C. D. Piazza, G. L. Tona, M. Luna and M. Pucci, "Analytical Formulation of a Maximum Torque per Ampere (MTPA) Technique for SynRMs Considering the Magnetic Saturation," in IEEE Transactions on Industry Applications, vol. 56, no. 4, pp. 3846-3854, July-Aug. 2020, doi: 10.1109/TIA.2020.2993525.

[23] M. M. Chowdhury, M. E. Haque, S. Saha, M. A. Mahmud, A. Gargoom and A. M. T. Oo, "An Enhanced Control Scheme for an IPM Synchronous Generator Based Wind Turbine With MTPA Trajectory and Maximum Power Extraction," in IEEE Transactions on Energy Conversion, vol. 33, no. 2, pp. 556-566, June 2018, doi: 10.1109/TEC.2017.2769126.

[24] Q. Liu and K. Hameyer, "High-Performance Adaptive Torque Control for an IPMSM With Real-Time MTPA Operation," in IEEE Transactions on Energy Conversion, vol. 32, no. 2, pp. 571-581, June 2017, doi: 10.1109/TEC.2016.2633302.

[25] K. Li and Y. Wang, "Maximum Torque per Ampere (MTPA) Control for IPMSM Drives Using Signal Injection and an MTPA Control Law," in IEEE Transactions on Industrial Informatics, vol. 15, no. 10, pp. 5588-5598, Oct. 2019, doi: 10.1109/TII.2019.2905929.

[26] T. Sun and J. Wang, "Extension of Virtual-Signal-Injection-Based MTPA Control for Interior Permanent-Magnet Synchronous Machine Drives Into the Field-Weakening Region," in IEEE Transactions on Industrial Electronics, vol. 62, no. 11, pp. 6809-6817, Nov. 2015, doi: 10.1109/TIE.2015.2438772.

[27] T. Sun, J. Wang and X. Chen, "Maximum Torque Per Ampere (MTPA) Control for Interior Permanent Magnet Synchronous Machine Drives Based on Virtual Signal Injection," in IEEE Transactions on Power Electronics, vol. 30, no. 9, pp. 5036-5045, Sept. 2015, doi: 10.1109/TPEL.2014.2365814.

[28] G. Liu, J. Wang, W. Zhao and Q. Chen, "A Novel MTPA Control Strategy for IPMSM Drives by Space Vector Signal Injection," in IEEE Transactions on Industrial Electronics, vol. 64, no. 12, pp. 9243-9252, Dec. 2017, doi: 10.1109/TIE.2017.2711507.

[29] T. Sun and J. Wang, "Extension of Virtual-Signal-Injection-Based MTPA Control for Interior Permanent-Magnet Synchronous Machine Drives into the Field-Weakening Region," in IEEE Transactions on Industrial Electronics, vol. 62, no. 11, pp. 6809-6817, Nov. 2015, doi: 10.1109/TIE.2015.2438772.

[30] T. -G. Woo, S. -W. Park, S. -C. Choi, H. -J. Lee and Y. -D. Yoon, "Flux Saturation Model Including Cross Saturation for Synchronous Reluctance Machines and Its Identification Method at Standstill," in IEEE Transactions on Industrial Electronics, vol. 70, no. 3, pp. 2318-2328, March 2023, doi: 10.1109/TIE.2022.3174233.

[31] Q. Chen, W. Zhao, G. Liu and Z. Lin, "Extension of Virtual-Signal-Injection-Based MTPA Control for Five-Phase IPMSM Into Fault-Tolerant Operation," in IEEE Transactions on Industrial Electronics, vol. 66, no. 2, pp. 944-955, Feb. 2019, doi: 10.1109/TIE.2018.2826473.

[32] Choi, S., Lee, W., Kang, A. et al. Accuracy improvement of maximum torque per ampere control for interior permanent magnet synchronous motor drives reflecting PM flux linkage variations. J. Power Electron. 23, 1678–1687 (2023).

[33] M. O. Sonnaillon, G. Bisheimer, C. De Angelo and G. O. García, "Online Sensorless Induction Motor Temperature Monitoring," in IEEE Transactions on Energy Conversion, vol. 25, no. 2, pp. 273-280, June 2010, doi: 10.1109/TEC.2010.2042220.

[34] S. Odawara *et al*., "Iron Loss Evaluation of Reactor Core With Air Gaps by Magnetic Field Analysis Under High-Frequency Excitation," in *IEEE Transactions on Magnetics*, vol. 51, no. 11, pp. 1-4, Nov. 2015, Art no. 8402404, doi: 10.1109/TMAG.2015.2442984.

ACKNOWLEDGEMENT

This work was supported in part by Key R&D Program of Zhejiang under Grant No. 2024SSYS0048, and in part by Yongjiang Laboratory.

Dongyang Li (S'17-M'20) received the B.S. degree from the China University of Mining and Technology, Jiangsu, China, in 2017, and the M.S. degree from Southeast University, Jiangsu, China, in 2020. He is currently a Ph.D. student of PEMC Group in University of Nottingham Ningbo China. His research interests include the advanced control strategies for motor system.

Shuo Wang (S'17-M'19) received Ph.D. degree in control science and engineering from Tongji University in 2019, Shanghai, China. From 2017 to 2018, he became a Visiting researcher with Power Electronics, Machines and Control Group (PEMC Group), University of Nottingham, Nottingham, U.K. From 2020 to 2024, he worked as senior research fellow and now he is currently working as an assistant professor in Nottingham Ningbo China Beacon of Excellence Research and Innovation Institute (CBI) in university of Nottingham, Ningbo, China (UNNC). His current research interests include high performance torque control, sensorless control and flux-weakening control used for permanent magnet synchronous machines, synchronous reluctance machines and permanent magnet-assisted synchronous reluctance machines.

Chunyang Gu Chunyang Gu (SM'23) received BSc degree from Harbin Institute of Technology in 2010, and PhD degree from Tsinghua University in 2015, both in Electrical Engineering. She had worked as a PostDoc Research Fellow with the Power Electronics, Machines and Control (PEMC) Research Group, University of Nottingham, UK, from 2015 to 2017. She joined Department of Electrical and Electronic Engineering, University of Nottingham Ningbo China, in 2017, as an assistant professor. She is currently an associate professor with the same department. She was appointed as a research professor in Advanced Electrical Machine Drive Research Center, Yongjiang Laboratory, Ningbo, China, in 2023. Her research interests include power electronics for transportation electrification, renewable energy and grid applications.

Yuli Bao received B.Eng. degree in electrical engineering and renewable energy systems from the University of Nottingham, Nottingham, U.K. in 2013. He received Ph.D. degree in electrical and electronic engineering from the University of Nottingham, Nottingham, U.K. in 2020. He is currently working as a research fellow at University of Nottingham Ningbo China. His main research interests include design and optimization of high-performance electrical machines for different applications.

Xiaochen Zhang received the master's degree from Harbin University of Science and Technology, Harbin, China, in 2006, and the Ph.D. degree from Harbin Institute of Electrical Technology, Harbin, in 2012. He is with the Advanced Electric Drive Centre, Yongjiang Laboratory, Ningbo China, and Nottingham Ningbo China Beacons of Excellence Research and Innovation Institute, University of Nottingham Ningbo China, Ningbo, China. His research interests include research on electromagnetic and thermal analysis on electrical machines, especially in permanent magnetic machines and high-speed machines.

Chris Gerada (Senior Member, IEEE) received the Ph.D. degree in the numerical modeling of electrical machines from the University of Nottingham, Nottingham, U.K., in 2005. He was a Researcher with the University of Nottingham, Nottingham, U.K., on high-performance electrical drives and on the design and modeling of electromagnetic actuators for aerospace application. Since 2006, he has been a Project Manager with GE Aviation Strategic Partnership, Cincinnati, OH, USA. In 2008, he was a Lecturer of electrical machines; in 2011, an Associate Professor; and in 2013, a Professor with the University of Nottingham. His research focuses on the design and modeling of high-performance electric drives and machines.

Prof. He Zhang (M'14-SM'18)) received his B.Eng. degree in Control Science and Engineering from Zhejiang University, China, in 2002. He obtained the MSc. and Ph.D. degree in electrical machines from The University of Nottingham, UK, in 2004 and 2009 respectively. After this he worked as a Research Fellow at the University and Director of BestMotion Technology Centre. He moved to University of Nottingham Ningbo China as Senior Research Fellow in 2014, promoted to Principal Research Fellow in 2016 and to Professor in 2020.